

Analysis of Sliding Match Offset Values for Calibration for Broadband Vector Network Analyzer Measurements

Laszlo Banyasz*, Lajos Nagy

*Department of Broadband Infocommunications and Electromagnetic Theory,
Budapest University of Technology and Economics,
Muegyetem rkp. 3., H-1111 Budapest, Hungary*

** Cross Computing Solutions - Engineering Radar Integration (XC-AC/ERI3-Bp)
Robert Bosch Ltd., Budapest, Hungary
laszlo.banyasz@edu.bme.hu*

Abstract. Efficient VNA calibration is crucial for accurate functional and EMC characterization of automotive radar antennas operating in the 76-77 GHz band. This paper presents a computationally efficient method for optimizing sliding match offset values during broadband calibration. Simulations and measurements validate the proposed approach, demonstrating improved accuracy and reduced calibration time for multi-channel MIMO radar applications.

1 Introduction

Ensuring electromagnetic compatibility (EMC) is paramount in today's increasingly complex electromagnetic environment, particularly with the proliferation of high-frequency devices. The automotive industry's rapid development depends on utilizing such components. [1]. For vehicular safety and autonomous driving, having automotive radars installed is considered a standard. These implement functions like automatic emergency braking or blind spot monitoring for safety, automatic cruise control, or other assets for driver's comfort [2].

Automotive radars operate in the 76-77 GHz frequency range. To achieve the required gain and antenna performance for these frequencies, manufacturers use *MIMO (Multiple Input – Multiple Output)* topologies [3][4][5]. The overall characteristics can be derived from the individual channel performance.

Generally, efforts are being made to reduce the length of connection and insertion losses. Also, the distance between radiating elements is comparable to the wavelength for antenna arrays [5]. This means these structures and their feed points are only a few millimeters apart. Based on this fact, performing measurements at this frequency is quite challenging.

Standard measurement methods include gain and pattern evaluation and input reflection measurement for such antennas. The latter is carried out via *VNA (Vector Network Analyzer)*. For the former case, scalar measurements are possible using a spectrum analyzer and an *RF (Radio Frequency)* generator—generally, VNAs in two-port mode are ideal for these kinds of measurements.

Calibration is a crucial part of VNA measurements. Therefore, a calibration plane has to be defined by executing a calibration procedure. The resulting scattering (S) parameters are referenced to this plane. For frequencies in the 70 GHz range, waveguides are usually used due to their low insertion loss—moreover, the space requirement is not significant. The WR-12 type is used for automotive radar applications with an operational frequency range of 60–90 GHz. In this regime, achieving a sufficiently ideal match standard emulating an infinitely long waveguide is not feasible. To be able to do a proper calibration, a so-called sliding match is used, the reflection coefficient of which magnitude is considered constant, and its phase angle can be varied by adjusting the physical distance of the internal absorber. The different reflection coefficient points are measured by recording multiple physical sliding match offsets, which lie on a circle in the complex impedance diagram. Performing these calibrations at a high level of precision, especially for MIMO measurements, can be time-consuming,

and these calibrations must be carried out frequently to ensure that the system meets its specifications. A typical calibration consists of three measurements, which are carried out using short, offset short and match standards. The sliding match adds a minimum of three but typically 4 to 8 extra measurement points, resulting in 7 to 11 measurements.

I. Kasa has proposed an efficient circle fitting method [6], which can be used for VNA sliding match calibration. I. Kasa performed a first-order random error analysis, and these error terms were evaluated for uniformly spaced data points and some nonuniform patterns. In case the circle-fitting is used for VNA sliding match calibration—the R&S manual states that this algorithm is employed during the calibration procedure [7]—it was also shown that the latter distributions could result in better broadband performance. At the same time, an analytical evaluation for such an optimal series “seems to be very difficult.”

2 Methodology

For a fixed frequency, a sequence of sliding match positions can be defined such that they are uniformly distributed on the complex impedance circle. Changing the frequency alters the phase shift introduced by the transmission line, causing these positions to shift according to the relationship between physical and electrical length. The phase shift of an ideal transmission line is:

$$\Phi = 2\beta D, \quad \text{where} \quad \beta = \frac{2\pi}{\lambda_g} \quad (1)$$

and the wavelengths of TEM [10] and TE₁₀ modes [11] are:

$$\lambda_{g, \text{TEM}} = \frac{c}{f\sqrt{\epsilon_e}} \quad \text{and} \quad \lambda_{g, \text{TE}_{10}} = \frac{\lambda_{\text{fs}}}{\sqrt{1 - \left(\frac{\lambda_{\text{fs}}}{2a}\right)^2}}, \quad (2)$$

where λ_{fs} is the free space wavelength, a is the width of the rectangular waveguide, ϵ_e is the effective dielectric constant.

Based on the frequency span, it could happen that a given physical distance distribution results in clumped or overlapping points, which, in addition to the measurement noise, results in ambiguously fitted circles. Celestino et al. [8] have already described these cases and provided an analytical analysis for rejecting data points that could result in inaccurate fitting. However, no investigation was carried out for optimally spaced uniform and nonuniform series for a given frequency span for different types of transmission lines.

Also, Celestino’s rejection algorithm tends to keep uniform point distributions along the circle, while theoretically, three well-chosen points could result in a good circle fit. Given the complexity of the nonuniform case, a straightforward approach would be to perform numerical simulations.

2.1 Direct Numerical Model

A sliding match distance distribution is given in the following way:

$$\mathbf{d} = \{d_i \mid d_i \geq 0, i \in \{1, 2, \dots, N\}, N \geq 3\}. \quad (3)$$

We divide a frequency span defined by f_{start} and f_{end} to M points:

$$f_j = f_{\text{start}} + (j - 1)\Delta f, \quad 1 \leq j \leq M, \quad (4)$$

where

$$\Delta f = \frac{f_{\text{end}} - f_{\text{start}}}{M - 1}. \quad (5)$$

We can define the following matrix:

$$\mathbf{\Phi} = (\Phi_{ij})_{N \times M}, \quad \text{where } \Phi_{ij} = \mathcal{P}(d_i, f_j) \quad \text{and} \quad \mathcal{P} \in \{\mathcal{P}_{\text{TEM}} \mid \mathcal{P}_{\text{TE10}}\}, \quad (6)$$

and the \mathcal{P} operator returns the corresponding phase shift for a given physical distance while the subscript indicates the transmission line type.

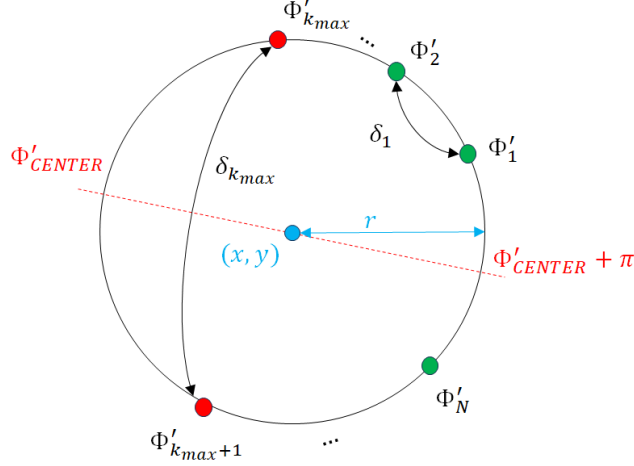


Figure 1: For a given f_j , the Φ'_i points on the circle are illustrated for the *Phase difference evenness* metric's penalty function. The center coordinates are (x, y) , and the radius is r . The Φ'_{center} is derived from the δ_k -s.

We define \mathcal{K} as Kasa's circle fitting operator, which returns the center coordinates x_j and y_j and the radius r_j of the fitted circle for each f_j frequency:

$$(x_j, y_j, r_j) = \mathcal{K}(\Phi_{1j}, \Phi_{2j}, \dots, \Phi_{Nj}), \quad (7)$$

$$(\mathbf{x}, \mathbf{y}, \mathbf{r}) = \mathcal{K}(\mathbf{\Phi}). \quad (8)$$

Where $\mathbf{x}, \mathbf{y}, \mathbf{r}$ are M long vectors. The measurement produces an estimator denoted as $\hat{\mathbf{\Phi}}$:

$$\hat{\mathbf{\Phi}} = \arg(e^{j\mathbf{\Phi}} + \mathbf{W}), \quad \text{where } \mathbf{W} = (W_{ij})_{N \times M}, \quad W_{ij} \in \mathbb{C}. \quad (9)$$

\mathbf{W} is a complex *noise* matrix. We will assume \mathbf{W} is Gaussian and the following is true:

$$\mathbb{E}(W_{ij}) = \mathbf{0} \quad \text{and} \quad \text{Var}(\Re(W_{ij})) = \text{Var}(\Im(W_{ij})) = \sigma^2, \quad \forall i, j. \quad (10)$$

The goal can be defined in the following way:

$$\min_{\mathbf{d}} \mathcal{Q}\{[\mathcal{K}(\arg(e^{j\mathcal{P}(\mathbf{d}, \mathbf{f})} + \mathbf{W}))]\}_p, \quad p \in (1, 2, 3), \quad (11)$$

where \mathcal{Q} is a cumulative statistical operator, which could represent the expected value or standard deviation of the cumulated vector. The p subscript represents one of the resulting circle parameters.

The numerical realization of \mathcal{Q} means that the minimization argument in Eq. (11) has to be evaluated for many \mathbf{W} realizations (Monte-Carlo simulation [9]). It is already a demanding task for a given \mathbf{d} ; hence, the minimization process becomes computationally inefficient.

2.2 Indirect Models

Instead of numerically evaluating a stochastic process, it would be more efficient to qualify a given \mathbf{d} sequence based on the Φ itself, which can be expressed the following way:

$$\zeta = \mathcal{M}(\Phi). \quad (12)$$

The circle fitting usually becomes problematic whenever the data points are clumped together in one or two clumps. \mathcal{M} is a metric function, which considers these behaviors; the resulting ζ quality value can be used to evaluate different \mathbf{d} sequences.

Many possible realizations exist for the \mathcal{M} metric operator. For these evaluations we create Φ' by wrapping and ordering the phases in Φ :

$$\Phi'_{ij} = \Phi_{ij} \pmod{2\pi}, \quad (13)$$

$$\Phi'_{i,j} \leq \Phi'_{i+1,j}, \quad \forall i, j. \quad (14)$$

Then we can define the phase difference matrix δ :

$$\delta_{kj} = \Phi'_{k+1,j} - \Phi'_{k,j}, \quad 1 \leq k \leq N-1, \quad (15)$$

$$\delta_{Nj} = \Phi'_{1,j} + 2\pi - \Phi'_{N,j}. \quad (16)$$

- *Cumulative phases* — Based on [8], one possible metric is to detect whether the points form a single clump:

$$\zeta_1(f_j) = 2\pi - \max_k \delta_{kj}. \quad (17)$$

$\zeta_1(f_j)$ is the largest phase difference between the wrapped data points. While this metric is small when the points are clumped, the behavior is linear-fashioned, so it cannot provide enough penalty for optimization purposes. Also, it does not punish when the dataset is focused on two points.

- *Phase difference evenness* — The following metric calculates the squared error of δ compared to the evenly distributed case:

$$\zeta_{2,A}(f_j) = \sqrt{\frac{1}{N-1} \sum_{k=1}^{N-1} \left(1 - \frac{\delta_{kj}}{2\pi/N}\right)^2}. \quad (18)$$

Favoring evenly distributed point sets means that point distributions with a smaller order than N will be penalized, while having at least three clusters could result in a good circle fit. This metric does not severely penalize focusing on two points.

Applying a proper penalty function could resolve the latter issue. Let us consider the following:

$$\hat{k}_j : \max_k \delta_{kj}, \quad (19)$$

$$\Phi'_{\text{center}} = \begin{cases} \frac{\Phi'_{\hat{k}_j+1,j} + \Phi'_{\hat{k}_j,j}}{2}, & \text{if } 1 \leq \hat{k}_j \leq N-1 \\ \frac{\Phi'_{1,j} + \Phi'_{N,j} + 2\pi}{2} \pmod{2\pi}, & \text{elsewhere.} \end{cases} \quad (20)$$

Φ'_{center} is the absolute middle phase point of the biggest wrapped phase difference. This way, we can define a penalty function (Eq. (21), (22)), which approaches infinity when the points are concentrated around $\Phi'_{\hat{k}_j}$ and $\Phi'_{\hat{k}_j+1}$. By definition, this is only possible, if $\delta_{\hat{k}_j} \geq \pi/2$:

$$\zeta_{2,P}(f_j) = \frac{1}{\sqrt{\sum_a (\Phi'_{\hat{k}_j,j} - \Phi'_{a,j})^2 + \sum_b (\Phi'_{\hat{k}_j+1,j} - \Phi'_{b,j})^2}}, \quad (21)$$

$$\forall a : \Phi'_{a,j} \geq \Phi'_{\text{center}} + \pi \quad \text{and} \quad \forall b : \Phi'_{b,j} < \Phi'_{\text{center}} + \pi, \quad a, b \in (1, \dots, N). \quad (22)$$

Using the penalty function, the resulting metric would be:

$$\zeta_2 = \zeta_{2,A} \zeta_{2,P}. \quad (23)$$

- *Polygonal area* — Another approach could consider the area of the inscribed polygon defined by the data points. The area approaches zero in the following cases: 1) Data points are concentrated around a single point; 2) data points are concentrated around two points. Similarly to the previous case, the area is smaller when clustering happens to the $(N-1)$ th degree. A unique normalization must be carried out if we want to compare results between different N values. The area is defined as a function of the phases:

$$\zeta_3(f_j) = \mathcal{A}(\Phi'_{1,j}, \Phi'_{2,j}, \dots, \Phi'_{N,j}). \quad (24)$$

- *Triangular area* — Since for circle fitting we require three properly spaced points, it is logical to consider all of the possible combinations and find the maximum area of the triangle:

$$\zeta_4(f_j) = \max_{p,q,r} \mathcal{A}(\Phi'_{p,j}, \Phi'_{q,j}, \Phi'_{r,j}), \quad p, q, r \in (1, \dots, N), \quad \forall p, q, r : p \neq q \neq r \neq p. \quad (25)$$

The benefit is that if three properly placed points are available during optimization for broad frequency ranges, the d can be considered reasonable. Moreover, this metric is invariant of N , so we can compare results from different N 's.

3 Simulation

The direct numerical model and the metrics for the indirect models have been implemented using *MATLAB*. The triangular area metric was modified according to Eq. (26), so it penalizes bad sequences:

$$\zeta'_4(f_j) = \frac{10}{\zeta_4(f_j) + 10^{-6}} - \frac{4 \cdot 10}{3\sqrt{3}}. \quad (26)$$

The behavior of the metrics is shown in Fig. 2; they were evaluated for a given uniform sequence and normalized. The peak is due to clustering around two points. Comparing them to the direct simulation, ζ_2 and ζ'_4 has a good rejection for this clustering. ζ_2 penalizes three-point clustering, not as much as two, but from the direct simulation result, we can conclude that only rejection for two-point clustering is important. Hence ζ'_4 was used for further evaluation.

3.1 Uniform distributions

First, uniform distributions were analyzed. For the TE10 waveguide case, Eq. (27) was considered due to the typical operation region – cutoff frequency relations for standardized waveguides. On the left side of Fig. 3, we can see that increasing the number of points lowers the metric and broadens the suitable sliding match spacing. To obtain these results, ζ'_4 was aggregated by taking its mean and/or deviation.

$$\frac{f_{\text{end}}}{f_{\text{start}}} = 1.5, \quad f_{\text{start}} = 1.25 \cdot f_{\text{cutoff}}. \quad (27)$$

The limitations in Eq. (27) do not apply to TEM. Hence, the same problem is optimized for different frequency spans. The required element spacing (almost) decreases monotonically while the corresponding errors grow. Using more points is especially beneficial at broad frequency ranges, while few points could give satisfactory results for small spans.

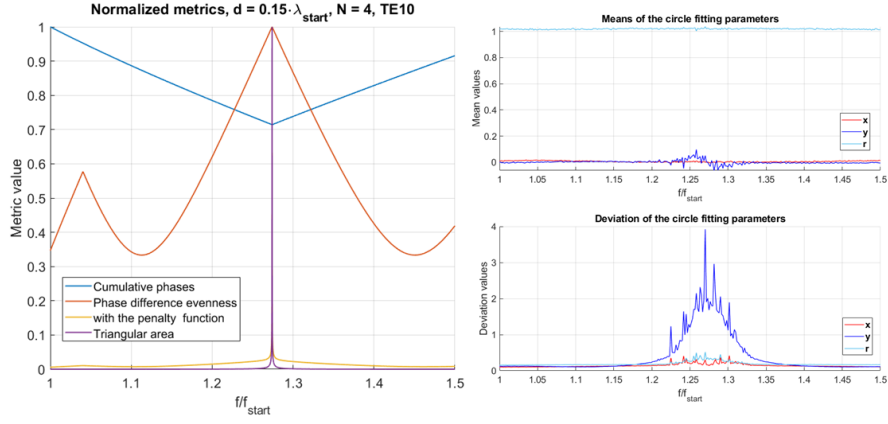


Figure 2: *Left*: normalized metrics of the indirect simulation; *Right*: direct numerical simulation, no. Monte-Carlo samples: 3000, $\sigma = 0.3$.

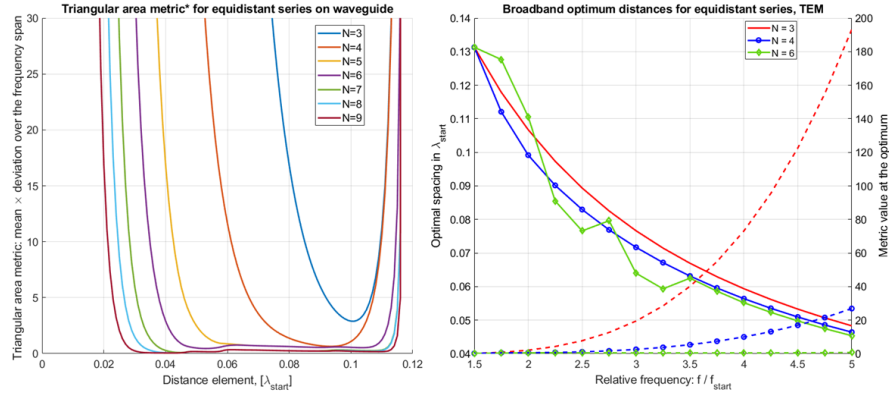


Figure 3: *Left*: optimal regions for uniform data distribution spacing for TE10 mode. The error is the product of the mean and deviation of the ζ'_4 ; *Right*: optimal spacing values (solid, left axis) for TEM mode transmission lines vs. the frequency span, and their corresponding errors (dashed, right axis). Mean of ζ'_4 was used for the optimization.

3.2 Nonuniform distributions

The numerical search for optimal nonuniform distributions was carried out with *MATLAB*'s *fmincon* function, using the interior-point algorithm. The objective function was the mean of ζ'_4 for the given frequency span. Using relative rather than absolute position values for the sliding match points, the required constraint equations were reduced. Thus we have got $(N-1)$ variables bounded $0 \leq d \leq U_b$, where we set $U_b = 2 \cdot \lambda_{\text{start}}$, because a few further spaced points might help with the performance.

The results of the numerical optimization procedure can greatly rely on the initial values depending on the objective function. For this case, the optimization was performed with multiple uniformly initialized vectors. The results were summarized in Tbl. (1). For a fixed number of points, it is clear from the results that increasing the frequency span increases the error metric. In other words, increasing the number of points for a given frequency span will result in a better circle fitting.

The optimization yielded uniform distribution for the $N = 3$ case, and the values were by Fig. (3).

4 Validation

Several measurements were carried out with a waveguide to validate the effectiveness of the chosen metric. The VNA was calibrated using a sliding match standard with an optimal $N = 9$ uniform

| Waveguide | | | | | | TEM $f_{end}/f_{start} = 1.5$ | | | | | |
|-----------------------------|-------|-------|-------|-------|-------|-------------------------------|-------|-------|-------|-------|-------|
| Metric | 2 | 3 | 4 | 5 | 6 | Metric | 2 | 3 | 4 | 5 | 6 |
| 0.375 | 0.123 | 0.216 | 0.296 | | | 0.202 | 0.041 | 0.157 | 0.288 | | |
| 0.375 | 0.080 | 0.173 | 0.296 | | | 0.202 | 0.116 | 0.247 | 0.404 | | |
| 0.742 | 0.094 | 0.210 | 0.412 | | | 0.472 | 0.131 | 0.196 | 0.261 | | |
| 0.191 | 0.085 | 0.167 | 0.195 | 0.313 | | 0.079 | 0.165 | 0.316 | 0.447 | 0.567 | |
| 0.224 | 0.084 | 0.174 | 0.292 | 0.407 | | 0.184 | 0.504 | 0.642 | 0.781 | 1.242 | |
| 0.230 | 0.121 | 0.210 | 0.244 | 0.294 | | 0.276 | 0.313 | 0.579 | 0.829 | 1.129 | |
| 0.162 | 0.136 | 0.220 | 0.247 | 0.305 | 0.347 | 0.062 | 0.137 | 0.285 | 0.323 | 0.448 | 0.569 |
| 0.206 | 0.339 | 0.445 | 0.551 | 0.635 | 0.678 | 0.065 | 0.232 | 0.392 | 0.546 | 0.676 | 0.798 |
| 0.211 | 0.180 | 0.226 | 0.308 | 0.433 | 0.633 | 0.110 | 0.641 | 0.793 | 0.921 | 1.042 | 1.578 |
| TEM $f_{end}/f_{start} = 3$ | | | | | | TEM $f_{end}/f_{start} = 5$ | | | | | |
| Metric | 2 | 3 | 4 | 5 | 6 | Metric | 2 | 3 | 4 | 5 | 6 |
| 0.629 | 0.062 | 0.131 | 0.241 | | | 1.228 | 0.041 | 0.095 | 0.184 | | |
| 0.629 | 0.110 | 0.179 | 0.241 | | | 1.228 | 0.089 | 0.142 | 0.184 | | |
| 0.690 | 0.141 | 0.226 | 0.292 | | | 1.284 | 0.104 | 0.183 | 0.248 | | |
| 0.309 | 0.079 | 0.147 | 0.196 | 0.311 | | 0.385 | 0.123 | 0.195 | 0.239 | 0.275 | |
| 0.310 | 0.060 | 0.123 | 0.203 | 0.293 | | 0.385 | 0.040 | 0.089 | 0.179 | 0.313 | |
| 0.368 | 0.110 | 0.182 | 0.247 | 0.399 | | 0.514 | 0.067 | 0.143 | 0.240 | 0.347 | |
| 0.161 | 0.154 | 0.217 | 0.281 | 0.307 | 0.397 | 0.214 | 0.108 | 0.153 | 0.197 | 0.222 | 0.293 |
| 0.207 | 0.115 | 0.230 | 0.292 | 0.364 | 0.452 | 0.221 | 0.074 | 0.100 | 0.146 | 0.195 | 0.310 |
| 0.220 | 0.173 | 0.338 | 0.394 | 0.489 | 0.623 | 0.301 | 0.093 | 0.171 | 0.239 | 0.361 | 0.482 |

Table 1: Simulation results for nonuniform distributions for TE₁₀ and TEM mode transmission lines. The elements are expressed in λ_{start} , starting from the 2nd up to 6 elements. The first element is always 0; hence not shown. The mean of ζ'_4 was used for the optimization.

series. ($d = 0.04 \cdot \lambda_{start}$, $\text{mean}\{\zeta'_4\} = 0.24$). Then, a separate fixed match standard, which was not involved in the calibration, was measured. The calibration was repeated but with different sliding match spacing series and N values. These results were compared by generating the difference to the reference complex S_{11} :

$$S_{\text{difference}} = 10 \cdot \log_{10}(|S_{11,ref} - S_{11,x}|). \quad (28)$$

A moving average filter with a length of 50 points was applied, and the results are shown on the left side of Fig. (3). Due to the significant magnitude difference in the metrics, their logarithm was plotted on the right side. The measurements prove that ζ'_4 correlates with error-prone points for the circle fitting—which is done by the integrated calibration algorithm of the VNA.

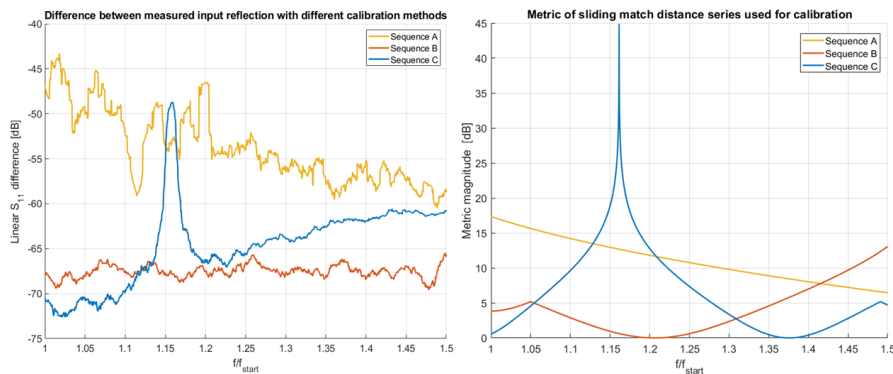


Figure 4: Measured differences due to errors from different calibration sequences and their evaluated metric's logarithm.

5 Conclusion

This paper presented a computationally efficient method for optimizing sliding match offset values in broadband VNA calibration, targeting automotive radar applications (70 GHz range). The devel-

oped metrics effectively predict calibration accuracy by analyzing the distribution of the phase shifts of the reflection coefficients; based on these, optimal offsets were numerically derived. Simulations and measurements validated the approach, demonstrating improved performance compared to uniform offsets by mitigating phase shift clustering and enhancing circle fitting accuracy. The results can reduce calibration times and improve EMC and antenna measurement workflows. Future work could include analytical investigations of nonuniform phase distributions for potential closed-form solutions.

References

- [1] Y. Yang et al., *A study on the electromagnetic compatibility of 79GHz automotive radar*, 2017 IEEE 5th International Symposium on Electromagnetic Compatibility (EMC-Beijing), Beijing, China, 2017, pp. 1-6, doi: 10.1109/EMC-B.2017.8260403.
- [2] H. L. Bloecher, J. Dickmann and M. Andres, *Automotive active safety & comfort functions using radar*, 2009 IEEE International Conference on Ultra-Wideband, Vancouver, BC, Canada, 2009, pp. 490-494, doi: 10.1109/ICUWB.2009.5288790.
- [3] J. Liu, C. Gu, F. Zhang, Y. Zhang and J. -F. Mao, *A 77 GHz FMCW Radar System for Versatile Consumer Applications*, 2020 IEEE MTT-S International Wireless Symposium (IWS), Shanghai, China, 2020, pp. 1-3, doi: 10.1109/IWS49314.2020.9360165.
- [4] J. Xu, S. Lin, Y. Huang and Z. Wang, *Design of Patch Antenna Array with Cavity Structure on Quartz Glass for Radar Applications*, 2022 IEEE 9th International Symposium on Microwave, Antenna, Propagation and EMC Technologies for Wireless Communications (MAPE), Chengdu, China, 2022, pp. 208-211, doi: 10.1109/MAPE53743.2022.9935188.
- [5] Q. Chen et al., *A 77 GHz Phased Array Antenna Based on Substrate-Integrated Waveguide*, in IEEE Antennas and Wireless Propagation Letters, vol. 22, no. 12, pp. 2979-2983, Dec. 2023, doi: 10.1109/LAWP.2023.3307221.
- [6] I. Kasa, *A circle fitting procedure and its error analysis*, in IEEE Transactions on Instrumentation and Measurement, vol. IM-25, no. 1, pp. 8-14, March 1976, doi: 10.1109/TIM.1976.6312298.
- [7] Rohde & Schwarz, *R&S ZNA User Manual 1178.6462.02*, Version 29, 2023
- [8] C. A. Corral and C. S. Lindquist, *On implementing Kasa's circle fit procedure*, in IEEE Transactions on Instrumentation and Measurement, vol. 47, no. 3, pp. 789-795, June 1998, doi: 10.1109/19.744352.
- [9] Kroese, D.P., Brereton, T., Taimre, T. and Botev, Z.I., *Why the Monte Carlo method is so important today*, in WIREs Comput Stat, 6: 386-392. June 2014, doi: 10.1002/wics.1314
- [10] Pozar, D.M. (2012) *Microwave Engineering*. 4th Edition, John Wiley & Sons.
- [11] Ramo, S., R. Whinnery, J., & Van Duzer, T. (1994). *Fields and Waves in Communication Electronics* (3rd ed.). John Wiley & Sons.

Acknowledgements – The author wishes to express his gratitude to Vince Obreczan and Anett Kenderes for their invaluable contributions in catalyzing the thought processes that shaped this work. The reported research was supported by the Doctoral Student Scholarship Program (Cooperative Doctoral Program, Ministry for Innovation and Technology, source of the National Research Development). We want to thank the Robert Bosch Ltd./Bosch Group, Hungary, for their professional support of the research that the study is based on.